Inorganic Chemistry

Article

pubs.acs.org/IC

$Ca_{10}Pt_7Tt_3$ (Tt = Si, Ge): New Platinide Phases Featuring Electron-Rich 4c–6e Bonded $[Pt_7Tt_3]^{20-}$ Intermetalloid Clusters

Isa Doverbratt,[†] Siméon Ponou,*[,†] Sven Lidin,[†] and Daniel C. Fredrickson[‡]

[†]Division of Polymer and Materials Chemistry, Lund University, Box 124, SE-221 00 Lund, Sweden

[‡]Department of Chemistry, University of Wisconsin—Madison, 1101 University Avenue, Madison, Wisconsin 53706, United States

Supporting Information

ABSTRACT: Two new phases $Ca_{10}Pt_7Tt_3$ (with Tt = Si, Ge) were obtained by reacting stoichiometric mixtures of the elements at high temperature. Their structures were refined from single crystal X-ray diffraction data. They are isostructural and crystallize in the $Ba_{10}Al_3Ge_7$ type structure, space group $P6_3/mcm$ (No. 193) with $a = b = 8.7735(3)$ Å, $c = 13.8260(5)$ Å, $V = 921.66(6)$ Å^3, $Z = 2$ for Tt = Si, and $a = b = 8.7995(6)$ Å, $c = 13.9217(14)$ Å, $V = 933.56(16)$ Å^3 for Tt = Ge phase. The most interesting structural features in these phases are the propeller shape $\{Pt_7Tt_3\}$ (Tt = Si, Ge) *intermetalloid* clusters in a D_{3h} local symmetry. LMTO electronic structure calculations and COHP analyses reveal that both $Ca_{10}Pt_7Tt_3$ (Tt = Si, Ge) phases are charge optimized, which is not predicted by the classical Zintl concept and the octet or Wade–Mingo's rules, but rather by a more complex bonding model based on the unprecedented electron-rich 4c–6e multicenter bonding. The clusters are best described as three-condensed trigonal planar $[TtPt_3]^{8-}$ units, resulting in a central Pt atom also with a trigonal planar coordination of three symmetrical equivalent Si/Ge atoms that are further connected to two terminal Pt atoms each. The "trefoil" electron-rich multicenter bonding is proposed here for the first time, and may be viewed as a unique bonding feature with potential relevance for the catalytic properties of the noble metal platinum.

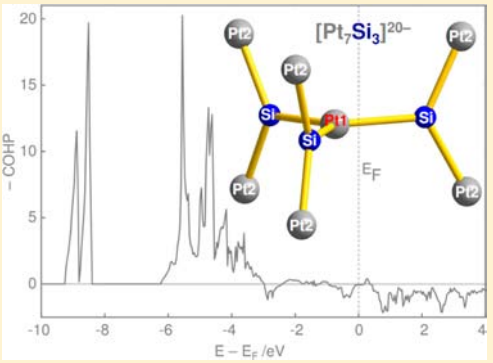

INTRODUCTION

The development of conceptual models for rationalizing the diversity or guiding the crystal structures of intermetallic compounds has remained very challenging, despite the very fast expansion of their rich structural chemistry, powered by an intense exploratory synthesis.[1] For intermetallic phases formed between elements with sufficiently large electronegativity differences, the Zintl concept, which is derived from the octet or the Wade–Mingos rules in molecular chemistry, postulates that the resulting structures will attain closed-shell electron configurations on the atoms through ionization and covalent bonds formation.[2,3] Borderline cases of Zintl phases, that is, those that exhibit "locally delocalized electrons" and do not conform to the Zintl–Klemm concept in it classical sense, mark the transition to the intermetallic phases. For these, successive reformulations of Zintl concept have been proposed, aiming at finding applicable "electron counting rules" by using analogies to appropriate bonding concept known from molecular chemistry.[4−6]

A closely related issue is to extend the Zintl concept to transition metals (TMs), and this has been first addressed by assuming the transition metal acts as an electropositive constituent. Thus, the term transition metal Zintl phase was introduced, referring to transition metal containing compounds that are either isostructural to classical main group metalloid Zintl compounds or to new TM structures, where the Zintl formalism provides insight into the electronic structure and bonding.[3,7] However, with the support of theoretical band structure calculations, recent reports have revealed that the TMs may be present also in negative oxidation state, thereby acting as a pseudo-p-block element. This is particularly true for the late TMs with completely filled d^{10}-orbitals including noble metals like Pd, Ag, Pt, or Au.[6,8−10] Nevertheless, it is still virtually impossible to apply simple heuristic concepts to reliably deduce compositions, structural features, or the nature of the bonding of this class of materials. Therefore, the rationalization of their synthesis remains the most challenging among inorganic compounds.[11,12] One possible approach to design new intermetallic phases featuring TM anions may be based on a phase diagram analogy with main group Zintl phases.

While a partial phase diagram analogy is quite common in the intermetallic realm, complete phase analogy is close to nonexistent. Understanding why two different systems often yield a similar chemical composition and/or structural feature is very important to explain atomic order in intermetallic phases. In this context, singular structures, i.e., having unique representatives, are likely to display novel bonding requirements and/or feature unique structural motives.[13,14] A nice representative of exclusive structure is the phase $Ba_{10}Al_3Ge_7$[14] which is one electron excessive according to the Zintl concept,

Received: August 28, 2012
Published: October 22, 2012

   dx.doi.org/10.1021/ic301867q | *Inorg. Chem.* 2012, 51, 11980–11985

and features $[Al_3Ge_7]^{19-}$ clusters consisting of trifold coordinated Al atoms having one vacant orbital (Lewis acid) and mixed-valent Ge atoms (3- and 2-fold coordinated).

As part of our research efforts to understand the structure directing forces and chemical bonding in ternary transition (noble) metal Zintl phases, we were able to achieve synthesis of the new phases $Ca_{10}Pt_7Tt_3$ (Tt = Si, Ge) which are isostructural but not isoelectronic with $Ba_{10}Al_3Ge_7$. We report herein on their synthesis, crystal structures, as well as bonding analysis based on first principle DFT band structures calculations.

EXPERIMENTAL SECTION

Synthesis and Characterization. All manipulations of the starting materials and products were done in an argon-filled glovebox with O_2 and H_2O level <0.1 ppm. For the synthesis, stoichiometric mixtures of the elements (ABCR GmbH, Karlsruhe, Germany) Ca (granules, 99.5%), Pt (plates, 99.9%), Ge (50 μ, 99.999%), and Si (powder, 99.999%+) were loaded in a niobium ampules which were sealed on both ends by arc-melting and, in turn, enclosed in an evacuated fused silica Schlenk tube to protect from air oxidation at high temperature. The compounds $Ca_{10}Pt_7Tt_3$ (Tt = Si, Ge) were obtained by heating at 1000 °C/24 h followed by slow cooling to room temperature at the rate of −6 °C/h; the reacted samples were routinely characterized by X-ray powder diffraction on a Stoe diffractometer (Ge(111) monochromator for Cu Kα_1 radiation: λ = 1.540 56 Å) equipped with a linear position sensitive (PSD) detector. According to the X-ray powder diffraction pattern, the reaction products were mixtures of the title phases with either small amounts of $Ca_3Pt_3Si_2$ phase ($Ce_3Rh_3Si_2$-type)[15] for the Si sample, or other yet unidentified phases for the Ge sample. Higher reaction time at 1000 °C does not seem to improve the reaction yield, particularly for Ge samples which produced single crystals of lower crystalline quality and higher amounts of byproducts.

EDS Analysis. The single crystals of the two phases were analyzed by the energy dispersive X-ray spectroscopy (EDS) technique using a field emission scanning electron microscope (JSM-7000F, JEOL, Japan) and equipped with an energy dispersive X-ray spectrometer (INCAx-sight, Oxford Instruments, U.K.). Elemental cobalt was used as standard, and corrections for atomic number, absorption, and fluorescence were applied. The analysis on several single crystals of the substituted phase confirmed the presence of all four elements with the atomic ratio Ca:Pt:Ge = 51(1):33(1):16(1), or Ca:Pt:Si = 55(1):30(1):15(1), close to the refined values. No other contaminant elements at the detection limit were observed.

Single Crystal Diffraction Studies. Several black, trigonal shaped crystals with metallic luster could be found in the reaction products and were attached at the tip of a glass fiber with glue and protected from oxidation in air by coating with Paratone N. Single crystal X-ray diffraction data of $Ca_{10}Pt_7Tt_3$ (Tt = Si, Ge) were collected at room temperature (293 K) on an Xcalibur3 diffractometer equipped with a CCD camera using Mo Kα radiation (λ = 0.710 73 Å) from an enhanced optic X-ray tube operating at 50 kV and 40 mA, and a detector-to-crystal distance of 50 mm. Data integration and numerical absorption corrections (multiscan) were carried out with the *Crysalis* software package.[16] Crystal data follow: hexagonal, $a = b$ = 8.7735(3) Å, c = 13.8260(5) Å, V = 921.66(6) Å^3 for the Si phase, and $a = b$ = 8.8059(5) Å, c = 13.890(1) Å, V = 932.78(11) Å^3 for the Ge phase. The space group $P6_3/mcm$ (No. 193), Z = 2, was indicated by the systematically absent reflections and confirmed by the successful structure solution and refinement with the SHELXTL software package.[17] Some relevant crystallographic data and refinement details are given in Table 1, while Table 2 contains the atomic positions and equivalent displacement parameters. Further details on the crystal structure investigations may be obtained from Supporting Information in CIF format. The structures were also deposit at the Fachinformationszentrum Karlsruhe, 76344 Eggenstein-Leopoldshafen, Germany (fax +49−7247808666; e-mail crysdata@fiz-karlsruhe.de), with the depository number CSD-424522 for $Ca_{10}Pt_7Si_3$ and CSD-424521 for $Ca_{10}Pt_7Ge_3$.

Theoretical Calculations. All electronic-structure calculations were based on the all-electron scalar relativistic tight binding linear muffin-tin orbital (TB-LMTO) theory.[18] Local density approximation (LDA) was used for the exchange correlation contributions to the total energy parametrization potential according to Barth and Hedin.[19] Self-consistency was achieved when the total energy change was smaller than 10^{-5} Ry. The chemical bonding situations were investigated using the crystal orbital Hamilton population (COHP)[20] technique as implemented in the TB-LMTO-ASA 4.7 program package.[21]

Table 1. Selected Crystal and Refinement Results Data

formula unit	$Ca_{10}Pt_7Si_3$	$Ca_{10}Pt_7Ge_3$
fw	1850.70	1984.20
cryst syst/space group	hexagonal/$P6_3/mcm$ (No. 193), Z = 2	hexagonal/$P6_3/mcm$ (No. 193), Z = 2
unit cell params	a = 8.7735(3) Å	a = 8.8059(5) Å
	b = 8.7735(3) Å	b = 8.8059(5) Å
	c = 13.826(1) Å	c = 13.890(1) Å
unit cell V	921.66(6) Å^3	932.78(11)
calcd density	6.669 g/cm^3	7.065
μ (Mo Kα, λ = 0.710 73 Å)	55.862 mm^{-1}	59.744
θmin/max	2.68/30.66	2.67/34.01
index ranges	$-11 \le h \le 9$, $-12 \le k \le 11$, $-19 \le l \le 18$	$-13 \le h \le 13$, $-11 \le k \le 13$, $-21 \le l \le 21$
collected reflns	4976 (R_σ = 0.0276)	17 119 (R_σ = 0.0880)
indep reflns	538 (R_{int} = 0.0439)	709 (R_{int} = 0.1562)
obsd reflns [$I > 2\sigma(I)$]	446	451
refinement method	full-matrix least-squares on F^2	full-matrix least-squares on F^2
params/restraints	24/0	24/0
GOF on F^2	1.034	0.905
final R indices [$I > 2\sigma(I)$]	R1 = 0.0235/wR2 = 0.0556	R1 = 0.0287/wR2 = 0.0476
final R indices (all data)	R1 = 0.0329/wR2 = 0.0580	R1 = 0.0799/wR2 = 0.0516
weighting scheme[a]	a = 0.0339	a = 0.0203
extinction coefficient	0.000 28(7)	0.000 09(3)
residual density (e$^-$/Å^3)	1.54/−2.66	2.429/−3.900

[a] $w = 1/[\sigma^2(F_o^2) + (aP)^2 + bP]$ where $P = (F_o^2 + 2 \times F_c^2)/3$.

Table 2. Atomic Coordinates and Equivalent Isotropic Displacement Parameters (U_{eq}[a])

atom	Wyck.	x	y	z	U_{eq}/Å^2
$Ca_{10}Pt_7Si_3$					
Pt1	2a	0	0	1/4	0.0086(2)
Pt2	12k	0	0.40799(4)	0.09736(2)	0.0098(1)
Si1	6g	0	0.2852(5)	1/4	0.0098(8)
Ca1	12k	0	0.7422(2)	0.1062(1)	0.0100(4)
Ca2	4d	1/3	2/3	0	0.0093(6)
Ca3	4c	2/3	1/3	1/4	0.0131(7)
$Ca_{10}Pt_7Ge_3$					
Pt1	2a	0	0	1/4	0.0116(3)
Pt2	12k	0	0.4148(1)	0.0908(1)	0.0098(1)
Ge1	6g	0	0.2930(2)	1/4	0.0096(3)
Ca1	12k	0	0.7464(3)	0.1064(2)	0.0106(5)
Ca2	4d	1/3	2/3	0	0.0087(8)
Ca3	4c	2/3	1/3	1/4	0.0154(9)

[a] U_{eq} is defined as one-third of the trace of the orthogonalized U^{ij} tensor.

dx.doi.org/10.1021/ic301867q | *Inorg. Chem.* 2012, 51, 11980−11985

RESULTS AND DISCUSSION

The title compounds $Ca_{10}Pt_7Tt_3$ (Tt = Si, Ge) were obtained by direct combination of the elements in stoichiometric proportions at high temperature. The chemical compositions of the air-sensitive crystals were confirmed by EDX analysis, and no impurity elements were detected. Their crystal structures were determined by single-crystal X-ray diffraction. They crystallize in a $Ba_{10}Al_3Ge_7$ type structure[14] with Ca at Ba positions, Pt at Ge positions, and Si/Ge atoms at Al positions. There are three, two, and one Ca, Pt, and Si positions in the unit cell, respectively. The "isolated" $[Pt_7Tt_3]$ propeller shaped intermetalloid clusters (Tt = Si, Ge) with D_{3h} local symmetry are embedded in a matrix of Ca atoms (Figure 1). Two

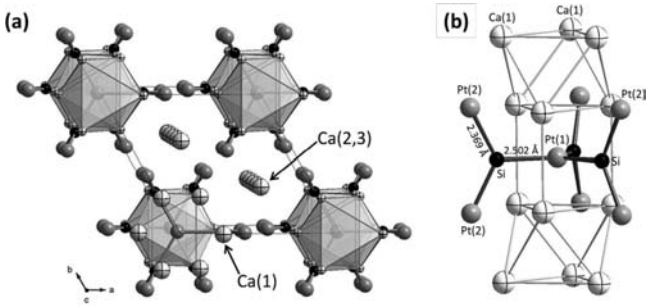

Figure 1. (a) Projection of the structure of $Ca_{10}Pt_7Si_3$ along [001] with polyhedral representation of Ca(1) octahedra. (b) Detailed view of the local structure of $[Pt_7Si_3]$ intermetalloid cluster with Si–Pt bond lengths and Ca(1) surrounding.

different Pt–Si/Ge distances (Table 3) are observed within the clusters: Pt1–Si1 = 2.502 Å (2.580(2) for Ge) comparable to the sum of the respective atomic radii[22] of Pt (1.37 Å) and Si (1.17 Å) or Ge (1.22 Å), and Si1–Pt2 = 2.370 Å (2.458(1) Å for Ge) which is significantly shorter than the sum of atomic radii. This suggests strong bonding interactions within the clusters. The shortest distance between two $[Pt_7Tt_3]$ clusters corresponds to Pt2–Pt2 = 3.139(1) Å (or 2.935(1) Å for the Ge phase), and represent weak secondary interactions. The shortening of the intercluster contact going from Si to larger Ge may be ascribed to chemical pressure, resulting from the increase of the cluster volume in the same Ca matrix. This is an indication that the intercluster distance is essentially determined by packing factors.

The calcium substructure is characterized by chains of interconnected Ca_6 empty octahedra formed by Ca1 atoms and running in the *c*-direction. The connections of these octahedra define trigonal prisms that are centered by the Pt1 atoms of the clusters. The three lateral faces of these trigonal prisms are capped by Si atoms. Ca2 and Ca3 form linear chains running along the *c*-direction. All Ca–Ca distances are larger than 3.4565(1) Å, which is consistent with those observed in other Ca tetrelide structures.[23]

Similar trigonal planar coordination of Si by Pt atoms, and vice versa, is found in LaPtSi with Si–Pt bond distances of 2.412 and 2.451 Å,[24] clearly intermediate to the bond distances observed in the title compounds. Interestingly enough, mixed metal phosphide-oxide phases, $Na_3M_7(P_3)_3O$ (M = Sr, Eu) that are isopointal to $Ca_{10}Pt_7Tt_3$, were reported previously by von Schnering et al.[25] with oxygen atoms located at the center of the M_6 octahedra, and empty trigonal M_6 prisms. These phases are characterized by "isolated" P_3^{5-} polyanions, with three of them replacing the (Pt_7Si_3) cluster, and the central Pt1 position (center of the Ca_6 octahedra) unoccupied.

Unlike the prototype $Ba_{10}Al_3Ge_7$ or the isopointal phase $Na_3M_7(P_3)_3O$ which could be described as Zintl phase, the rationalization of the bonding in compounds $Ca_{10}Pt_7Tt_3$ with the Zintl concept seems at first challenging. Therefore, to understand the structure directing forces at work here, we conducted DFT band structure calculations. The densities of states (DOS) plots of the two phases with projected DOS (PDOS) of the three different components (Ca, Pt, Tt = Si/Ge), obtained by the LMTO method, are virtually identical as seen in Figure 2, and therefore we will focus on the phase $Ca_{10}Pt_7Si_3$ as one representative. There is no energy gap at the Fermi level, but a distinct minimum of the DOS (pseudogap), and the compounds are predicted to be poor metals. The relatively deep pseudogap at E_F is an indication that the compound $Ca_{10}Pt_7Si_3$ is electronically stable, and the absence of a real gap may be attributed to incomplete charge transfer from Ca to the anionic network as usually observed in Ca tetrelide phases.[23] The analysis of the chemical bonding in $Ca_{10}Pt_7Si_3$ using the COHP[20] method and its energy integral (ICOHP) clearly indicates that the Si–Pt interatomic contacts within the $[Pt_7Si_3]$ clusters are strongly bonding and well optimized interactions, with a real energy gap at E_F separating the occupied bonding and nonbonding states with the unoccupied antibonding levels (Figure 3). At first glance, this cannot be predicted by using the Zintl concept and the 8-N or the Wade–Mingos rules.

We assume a full electron transfer from calcium to the more electronegative Pt and Si (or Ge) atoms, according to the Zintl concept,[2] results in the ionic formulation $(10Ca^{2+})[Pt_7Tt_3]^{20-}$. Since a maximum of 12 electrons are needed to achieve a full octet for the 3 tetrel atoms, one has to assume that the Pt atoms in the clusters are in negative oxidation states. This means that the remaining 8 electrons should be at least partially distributed to the 7 Pt atoms. An isolated Pt^{2-} anion corresponds to a close shell species like He, and was observed in the compound Cs_2Pt which shows typical physicochemical

Table 3. Calculated −ICOHP Values [eV/bond] of Relevant Interatomic Distances in $Ca_{10}Pt_7Tt_3$ (Tt = Si, Ge)[a]

		Tt = Si		Tt = Ge	
atom pair	*n*	length [/Å]	−ICOHP	length [/Å]	−ICOHP
Pt1–Tt1	(×3)	2.502(4)	2.86	2.580(2)	2.564
Si1–Pt2	(×2)	2.369(2)	3.45	2.458(1)	3.055
Pt2–Pt2	(×1)	3.139(1)[b]	0.88	2.935(1)[b]	1.381
Pt1–Ca1	(×6)	3.011(2)	0.70	2.994(2)	0.719
Pt2–Ca1,2	(×8)	2.935(2),−3.394(1)	0.74	2.928(2),−3.452(1)	0.723
Si1–Ca1,3	(×6)	3.109(2),−3.157(4)	0.57	3.128(1),−3.140(2)	0.572

[a] *n* is the frequency of interactions for the given bond. [b] Corresponds to intercluster distances.

dx.doi.org/10.1021/ic301867q | Inorg. Chem. 2012, 51, 11980–11985

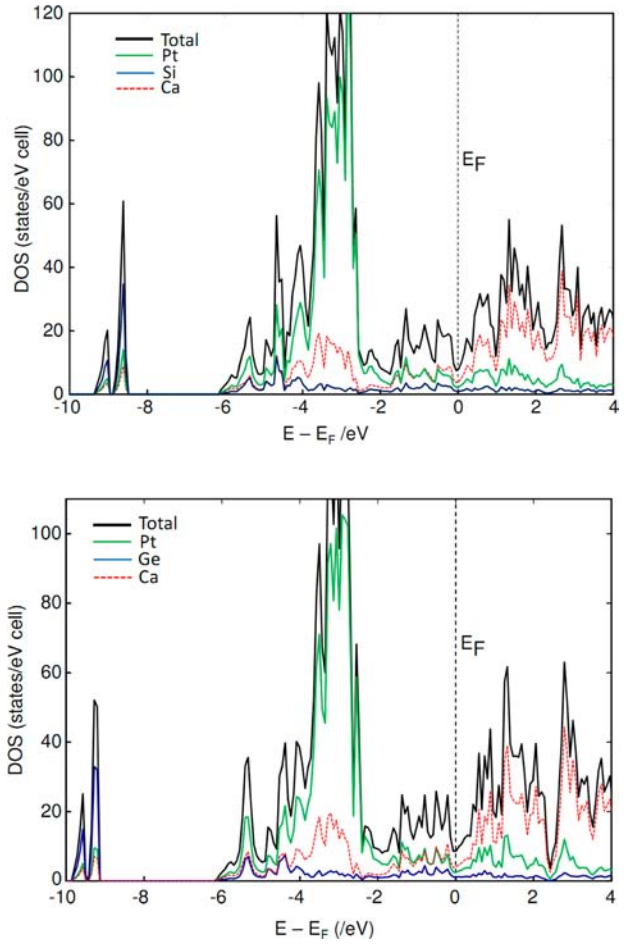

Figure 2. Calculated DOS (and PDOS) plots for the $Ca_{10}Pt_7Si_3$ (top) and $Ca_{10}Pt_7Ge_3$ (bottom) phases using the LMTO method.

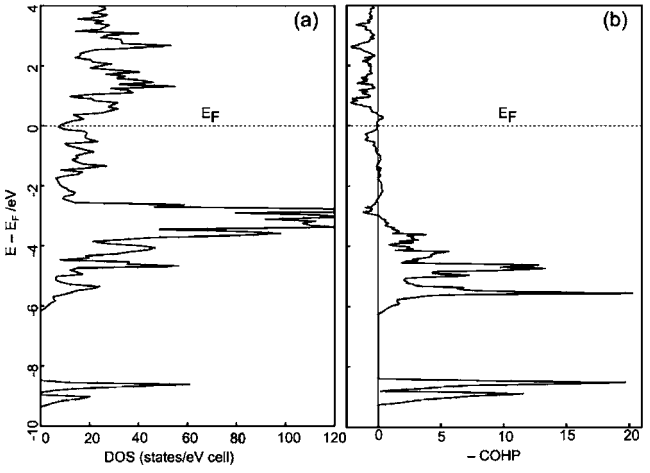

Figure 3. (a) Theoretical DOS plot for $Ca_{10}Pt_7Si_3$ and (b) COHP curve of all Pt–Si interactions within the $\{Pt_7Si_3\}$ cluster. The Fermi level (E_F) has been set to zero energy.

characteristics of an ionic compound.[9] In the case of $Ca_{10}Pt_7Si_3$, projected DOS analysis indicates that the sharp peaks between −4 and −2 eV are essentially contributed by the Pt-d orbitals meaning that there are localized and completely filled Pt-d^{10} orbitals and may be viewed as pseudocore. These Pt-d orbitals are also not visible in the −COHP curve, confirming that they are nonbonding orbitals. Further, strong Pt-s orbital contributions to the DOS also appear between −6 and −2.5 eV below the Fermi level as expected for negatively charged Pt atoms.

An arbitrary formal charge assignment would be to assume the six terminal Pt2 atoms as single charge atoms, i.e., Pt^-, and the central Pt1 (3-fold connected) as a double charge, i.e., Pt^{2-}. Hence, the closed-shell Si^{4-} is hypercoordinated by three Pt atoms meaning that the Si–Pt bonds within the cluster are electron-rich bonds, previously referred to as hypervalent, a concept which is falling in desuetude today.[26] In this so-called "electron-rich multicenter bonding" model,[27] the propeller shape $[Pt_7Si_3]^{20-}$ cluster can be derived by condensing three units of the hypothetical $[Pt_3Si]^{8-}$ cluster with trigonal planar geometry (D_{3h} symmetry). The 12 valence electrons system $[Pt_3Si]^{8-}$ (assuming Pt-$5d^{10}$ as pseudocore) consists of two closed shell Pt^{2-} atoms and covalently bonded opened shell Pt^{1-} and Si^{3-} atoms. The bonding of these units corresponds to an electron-rich four-center–six-electron (4c–6e) bond. One electron bonding pair is delocalized over all the three Pt–Si contacts by resonance. The Lewis diagram of this "trefoil" 4c–6e bonding system is schematically given in Figure 4. In

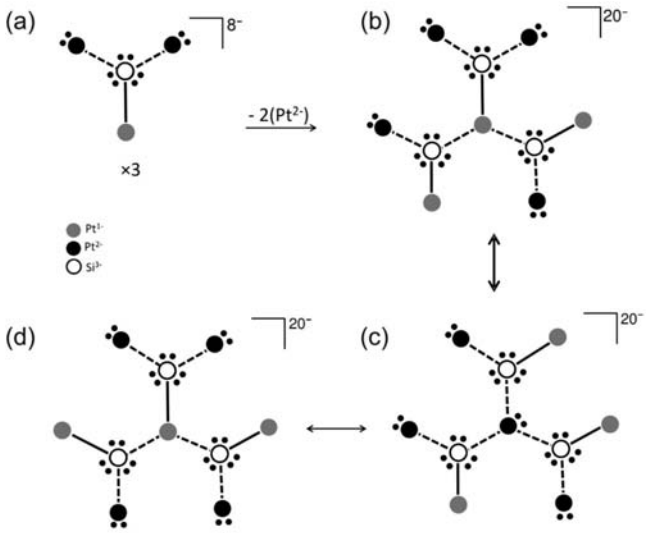

Figure 4. Lewis diagrams of (a) the hypothetical $[Pt_3Si]^{8-}$ cluster with electron-rich 4c–6e multicenter bonding and its condensation into (b) larger $[Pt_7Si_3]^{20-}$ cluster. (c, d) Further representatives of the resonance structures are shown, where dashed lines show the direction of interactions and continuous lines represent the bonding pair of electrons.

comparison, 3c–4e bonded systems[27] like ClF_3 are known to adopt a T-shape structure. Other prominent trigonal planar AX_3 units reported in intermetallic phases include the 24 valence electron systems $[SiPn_3]^{5-}$ (Pn = P, As) that were observed in the phases A_5SiPn_3 (A = Rb, Cs).[28] The isotypic and isoelectronic $[AgSn_3]^{11-}$ unit was also observed in $Li_{17}Ag_3Sn_6$.[29] These units are analogues of the aromatic carbonate anion $[CO_3]^{2-}$ or BF_3 known in molecular chemistry. Interestingly, the hypothetical 6-electron system $[SiPt_3]^{2-}$ would represent an analogue of BH_3 or CH_3^+. Further trigonal planar moieties are the 26-electron $[Tt_4]^{10-}$ homonuclear oligomers (Tt = Si, Ge) found in the compound $Ba_5Mg_{18}Si_{13}$ and its analogues.[30] They are isoelectronic to PF_3, which is nonplanar. To the best of our knowledge, no electron-rich multicenter bonded molecular unit with trigonal planar geometry has been described yet. The 120° bond angle

dx.doi.org/10.1021/ic301867q | Inorg. Chem. 2012, 51, 11980–11985

between the central Si/Ge and the terminal Pt atoms is also found in the trigonal bipyramidal structure like PCl_5 (D_{3h}), but here only the axial bonds are involved in the linear 3c−4e bonding type.

It is noteworthy, with the atomic coloring[12] issue, in electron-rich multicenter bonded systems the most electronegative atom is found at terminal positions as ligand, in order to pull away enough electrons from the hypercoordinated central atom to preserve the prevalence of the octet rule.[31] Therefore, the Pt is assumed to be more electronegative than Si and Ge, and this is true on the Pauling electronegativity scale with Pt (2.28), Si (1.90), and Ge (2.01). Moreover, the Pearson absolute electronegativity[32] also agreed with the atomic coloring of the cluster since Pt value (5.6 eV) is higher than Ge (4.6 eV) and Si (4.77 eV) values. This is the result of the far stronger relativistic effects in Pt atoms, and is probably a decisive factor for the unprecedented bonding picture in these clusters. From the projected DOS, the order of atomic orbital dominance in contribution to the DOS is roughly the following: Si-s < Pt-s < Pt-d, Si-p < Ca-s, Ca-d < Pt-p. This confirms the largest s−p orbital separation for Pt atoms, when compared to Si atoms. A reasonable formal charge assignment for the compound is therefore $(Ca^{2+})_{10}(Pt^{2-})_4(Pt^{1-})_3(Si^{3-})_3$. An alternative will consist of assigning the bonding electron pairs to silicon atoms, resulting in $(Ca^{2+})_{10}(Pt^{2-})_4(Pt^{0})_3(Si^{4-})_3$, but this is less consistent with the strong Pt−Si bonds observed in the structure.

Important enough, the linear 3c−4e molecular system XeF_2 is well-known to condense into square planar system XeF_4, a more extended delocalized bonding system. In the solid state, triatomic linear $[Pn_3]^{7-}$ units, analogues of XeF_2 or I_3^-, are ubiquitous and have been observed for all group 15 elements except nitrogen, in binary and ternary Zintl phases.[33] Their condensation into extended structures with various dimensionalities like 1D chains, strips, and ribbons or 2D square planes was described in binary and ternary phases of heavier pnictogens, Sb and Bi.[4,5] The condensation of the 3c−4e bonded system generally takes place on the central atom, but the three-condensed propeller shape $[Pt_7Tt_3]^{20-}$ cluster is realized rather by condensation on one of the terminal Pt atoms.

From the corresponding Lewis structure depicted in Figure 4, the propeller shape $[Pt_7Si_3]^{20-}$ clusters (32 valence electrons system) have 20 resonance structures as deduced from direct counting. This implies higher stability for the larger cluster compared to the simple $[SiPt_3]^{8-}$. Three over seven Pt atoms of $[Pt_7Si_3]^{20-}$ are covalently bonded to the Si atoms simultaneously according to the resonance model. The three bonding pairs of electrons should be distributed evenly relative to the silicon atoms to the nine Si−Pt directions of interaction. The −COHP curve indicates a wide nonbonding region expanding roughly between −3.0 eV and E_F, and according to the PDOS, they represent either localized Pt-d[10] electrons, or lone-pairs on Si atoms close to the Fermi level. The Si−Pt bonding levels are lower in energy, resulting in strong Si−Pt bonds as illustrated by the −ICOHP values listed in Table 3. In comparison, the values of the intercluster bonds are weak, in the same range as Ca−Pt interactions, and should represent secondary interactions.

Finally, in the 4c−6e bonding model described here, the frontier molecular orbitals consist of one bonding and two nonbonding filled levels, and this is fundamentally similar to the well-known 3c−4e bonding where one bonding and one nonbonding molecular levels are occupied, giving an average bond order of one for both systems.

CONCLUSIONS

The synthesis, crystal structures, and bonding rational of the phases $Ca_{10}Pt_7Tt_3$ (Tt = Si, Ge) have been investigated. They feature the propeller shape $[Pt_7Tt_3]^{20-}$ intermetalloid clusters in a D_{3h} local symmetry, and the rationalization of the bonding interactions in these clusters resulted in the unprecedented "trefoil" electron-rich 4c−6e multicenter bonding, in agreement with DFT calculations. No molecular analogue is known yet. Another interesting finding of the work is the relatively high electronegativity of the Pt atom in intermetallic compounds as well as its effect on the bonding and properties. One ultimate goal in intermetallic chemistry is to build up simple valence rules that may be used to predict their structure. In this context, the prominent work by Whangbo and Köhler[6] on transition metals in negative oxidation states has opened new horizons for more expansion of the Zintl concept to transition metal intermetallic compounds, as illustrated herein. Rationalizing the chemical bonding in intermetallic systems with noble metals like Pt is of high interest since most of the late transition metals and their alloys are important catalysts. Therefore, it is very important to fully understand their chemical behavior. Hence, the "trefoil" electron-rich 4c−6e multicenter bonding which is described here for the first time may be viewed as a unique bonding feature with potential relevance for the catalytic properties of the Pt noble metal.

ASSOCIATED CONTENT

Supporting Information

Detailed crystallographic data in CIF format, projected DOS for Pt1, Pt2 (s- and d-orbitals), and Si (s-, and p-orbitals) as well as −COHP (and −ICOHP) plots calculated for the Pt(1)−Si(1) and Pt(2)−Si(1) bonds in $Ca_{10}Pt_7Si_3$. This material is available free of charge via the Internet at http://pubs.acs.org.

AUTHOR INFORMATION

Corresponding Author

*E-mail: simeon.ponou@polymat.lth.se. Phone: (+46)46 222 4769. Fax: (+46)46 222 4012.

Notes

The authors declare no competing financial interest.

ACKNOWLEDGMENTS

This work was financially supported by the Swedish National Research Council (VR). S.P. thanks the Axel Wenner-Gren Foundation for a postdoctoral research fellowship.

REFERENCES

(1) Villars, P.; Calvert, L. D. *Pearson's Handbook of Crystallographic Data for Intermetallic Phases*, 2nd ed.; American Society for Metals International: Metals Park, OH, 1991.

(2) Schäfer, H.; Eisenmann, B.; Müller, W. *Angew. Chem., Int. Ed.* **1973**, *12* (9), 694.

(3) *Chemistry, Structure and Bonding of Zintl Phases and Ions*; Kauzlarich, S. M., Ed.; VCH Publishers: New York, 1996.

(4) (a) Papoian, G. A.; Hoffmann, R. *Angew. Chem., Int. Ed.* **2000**, *39*, 2409. (b) Papoian, G. A.; Hoffmann, R. *J. Am. Chem. Soc.* **2001**, *123*, 6600.

(5) Mills, A. M.; Lam, R.; Ferguson, M. J.; Deakin, L.; Mar, A. *Coord. Chem. Rev.* **2002**, *233*−*234*, 207−222 and the references therein.

(6) (a) Whangbo, M.-H.; Lee, C.; Köhler, J. *Angew. Chem., Int. Ed.* **2006**, *45*, 7465. (b) Köhler, J.; Whangbo, M.-H. *Solid State Sci.* **2008**, *10*, 444. (c) Köhler, J.; Whangbo, M.-H. *Chem. Mater.* **2008**, *20*, 2751.
(7) Kauzlarich, S. M.; Brown, S. R.; Snyder, G. J. *Dalton Trans.* **2007**, 2099−2107.
(8) Karpov, A.; Nuss, J.; Wedig, U.; Jansen, M. *J. Am. Chem. Soc.* **2004**, *126* (43), 14123−14128.
(9) (a) Karpov, A.; Jansen, M. *Angew. Chem., Int. Ed.* **2005**, *44*, 7639−7643; *Angew. Chem.* **2005**, *117*, 7813−7816. (b) Karpov, A.; Nuss, J.; Wedig, U.; Jansen, M. *Angew. Chem., Int. Ed.* **2003**, *42*, 4818.
(10) (a) Wedig, U.; Saltykov, V.; Nuss, J.; Jansen, M. *J. Am. Chem. Soc.* **2010**, *132*, 12458−12463. (b) Saltykov, V.; Nuss, J.; Wedig, U.; Jansen, M. *Z. Anorg. Allg. Chem.* **2010**, *636*, 2040.
(11) (a) Harris, N. A.; Hadler, A. B.; Fredrickson, D. C. *Z. Anorg. Allg. Chem.* **2011**, 1961−1974. (b) Fredrickson, D. C.; Lidin, S.; Venturini, G.; Malaman, B.; Christensen, J. *J. Am. Chem. Soc.* **2008**, *130*, 8195−8214. (b) Fredrickson, D. C.; Lee, S.; Hoffmann, R. *Angew. Chem.* **2007**, *119*, 2004−2022; *Angew. Chem., Int. Ed.* **2007**, *46*, 1958−1976.
(12) Miller, G. J. *Eur. J. Inorg. Chem.* **1998**, 523.
(13) Ponou, S.; Fässler, T. F.; Tobias, G.; Canadell, E.; Cho, A.; Sevov, S. C. *Chem.—Eur. J.* **2004**, *10*, 3615−3621.
(14) Widera, A.; Schäfer, H. *Z. Naturforsch.* **1977**, *B32*, 619−624. (b) Lin, J.; Hönle, W.; von Schnering, H.-G. *J. Alloys Compd.* **1992**, *178*, 455−465.
(15) Kaczorowski, D.; Prots, Yu.; Burkhardt, U.; Grin, Yu. *Intermetallics* **2007**, *15*, 225−232.
(16) Oxford Diffraction. *CrysAlis CCD and CrysAlis RED*; 2006; p171.31.2.
(17) (a) Sheldrick, G. M. *Acta Crystallogr., Sect. A* **2008**, *64*, 112. (b) *SHELXTL, version 5.1*; Bruker AXS Inc.: Madison, WI, 1998.
(18) (a) Andersen, O. K. *Phys. Rev. B* **1975**, *12*, 3060. (b) Skriver, H. *The LMTO Method*; Springer, Berlin, 1984.
(19) von Barth, U.; Hedin, L. *J. Phys. C: Solid State Phys.* **1972**, *5*, 1629−1642.
(20) Dronskowski, R.; Blöchl, P. *J. Phys. Chem.* **1993**, *97*, 8617.
(21) Krier, G.; Jepsen, O.; Burkhardt, A.; Andersen, O. K. *The TB-LMTO-ASA Program, version 4.7*; Max Planck Institute for Solid-State Research: Stuttgart, Germany.
(22) Donohue, J. *The Structures of the Elements*; Wiley: New York, 1974.
(23) (a) Ponou, S. *Eur. J. Inorg. Chem.* **2010**, 4139−4147. (b) Mudring, A.-V.; Corbett, J. D. *J. Am. Chem. Soc.* **2004**, *126*, 5277.
(24) Klepp, K.; Parthé, E. *Acta Crystallogr.* **1982**, *B38*, 1105−1108.
(25) Lin, J.; Hönle, W.; von Schnering, H.-G. *J. Alloys Compd.* **1992**, *178*, 455−465.
(26) von Ragué Schleyer, P. *Chem. Eng. News* **1984**, *62*, 4.
(27) (a) Pimentel, G. C. *J. Chem. Phys.* **1951**, *19*, 446. (b) Hach, R. J.; Rundle, R. E. *J. Am. Chem. Soc.* **1951**, *73*, 4321. (c) Musher, G. I. *Angew. Chem., Int. Ed.* **1969**, *8*, 54.
(28) (a) Eisenmann, B.; Klein, J.; Somer, M. *Angew. Chem.* **1990**, *102*, 92−93. (b) Eisenmann, B.; Klein, J.; Somer, M. *Z. Kristallogr.* **1991**, *197*, 273−274.
(29) Lupu, C.; Downie, C.; Guloy, A. M.; Albright, T. A.; Mao, J.-G. *J. Am. Chem. Soc.* **2004**, *126*, 4386−4397.
(30) Nesper, R.; Wengert, S.; Zurcher, F.; Currao, A. *Chem.—Eur. J.* **1999**, *5*, 3382.
(31) Mitchell, T. A.; Finocchio, D.; Kua, J. *J. Chem. Educ.* **2007**, *84*, 629.
(32) (a) Parr, R. G.; Pearson, R. G. *J. Am. Chem. Soc.* **1983**, *105*, 1503−1509. (b) Pearson, R. G. *Inorg. Chem.* **1988**, *27*, 734−740.
(33) (a) Cordier, G.; Schäfer, H.; Stelter, M. *Z. Anorg. Allg. Chem.* **1984**, *519*, 183−188. (b) Gallup, R. F.; Fong, C. Y.; Kauzlarich, S. M. *Inorg. Chem.* **1992**, *31*, 115−118. (c) Múnzarova, M. L.; Hoffmann, R. *J. Am. Chem. Soc.* **2002**, *124*, 4787.